2014-03

Molecular structure: optical property relationships for a series of non-centrosymmetric two-photon absorbing push-pull triarylamine molecules

Scientific Reports,London : Nature,v. 4, p. 4447-1-4447-11, Mar. 2014
http://www.producao.usp.br/handle/BDPI/50313

SCIENTIFIC REPORTS

OPEN

SUBJECT AREAS:
SPECTROSCOPY
NONLINEAR OPTICS

Received
21 January 2014

Accepted
7 March 2014

Published
24 March 2014

Molecular Structure – Optical Property Relationships for a Series of Non-Centrosymmetric Two-photon Absorbing Push-Pull Triarylamine Molecules

Marcelo G. Vivas[1,2], Daniel L. Silva[3,4], Jérémy Malinge[5], Mohammed Boujtita[8], Robert Zaleśny[6], Wojciech Bartkowiak[6], Hans Ågren[7], Sylvio Canuto[3], Leonardo De Boni[1], Eléna Ishow[5,8] & Cleber R. Mendonca[1]

Correspondence and requests for materials should be addressed to M.G.V. (mavivas82@yahoo.com.br) or C.R.M. (crmendon@ifsc.usp.br)

[1]Instituto de Física de São Carlos, Universidade de São Paulo, Caixa Postal 369, 13560-970 São Carlos, SP, Brazil, [2]Instituto de Ciência e Tecnologia, Universidade Federal de Alfenas, Cidade Universitária - BR 267 Km 533, 37715-400 Poços de Caldas, MG, Brazil, [3]Instituto de Física, Universidade de São Paulo, CP 66318, 05314-970, São Paulo, SP, Brazil, [4]Departamento de Ciências da Natureza, Matemática e Educação, Universidade Federal de São Carlos, Rod. Anhanguera – Km 174, 13600-970 Araras, SP, Brazil, [5]PPSM-UMR CNRS 8531, ENS Cachan, 61 avenue du Président Wilson, 94235 Cachan, France, [6]Theoretical Chemistry Group, Institute of Physical and Theoretical Chemistry, Wroclaw University of Technology, Wybrzeze Wyspianskiego 27, 50-370 Wroclaw, Poland, [7]Department of Theoretical Chemistry and Biology, School of Biotechnology, Royal Institute of Technology, SE-106 91 Stockholm, Sweden, [8]CEISAM–UMR CNRS 6230, Université de Nantes, 2 rue de la Houssinière, 44322 Nantes, France.

This article reports on a comprehensive study of the two-photon absorption (2PA) properties of six novel push-pull octupolar triarylamine compounds as a function of the nature of the electron-withdrawing groups. These compounds present an octupolar structure consisting of a triarylamine core bearing two 3,3′-bis(trifluoromethyl)phenyl arms and a third group with varying electron-withdrawing strength (H < CN < CHO < NO2 < Cyet < Vin). The 2PA cross-sections, measured by using the femtosecond open-aperture Z-scan technique, showed significant enhancement from 45 up to 125 GM for the lowest energy band and from 95 up to 270 GM for the highest energy band. The results were elucidated based on the large changes in the transition and permanent dipole moments and in terms of (i) EWG strength, (ii) degree of donor-acceptor charge transfer and (iii) electronic coupling between the arms. The 2PA results were eventually supported and confronted with theoretical DFT calculations of the two-photon transition oscillator strengths.

Comprehensive studies of the two-photon absorption (2PA) cross-section on a wide spectral range are of fundamental importance to understand, at the molecular level, the relation between the molecular structure and electronic and optical properties of novel organic materials. Due to its remarkable characteristics, such as the advantageous excitation in the near-IR region and the high spatial localization of excitation, the 2PA has been used in several kinds of applications including 3D optical data storage[1,2], fluorescence imaging[3–5], all-optical switching[6,7], optical power limiting[8–10], photodynamic therapy[11–13], frequency upconverted lasing[14], coherent control of molecular systems[15,16], microfabrication via photopolymerization[17,18], micromachining[19,20], to name a few.

In the last three decades, different types of molecules have been proposed as alternative molecular designs to improve nonlinear hyperpolarizabilities and decrease the irradiance threshold necessary to generate a specific nonlinear optical effect. Three main designs have been largely studied: the dipolar (A-π-D)[21–23], quadrupolar (A-π-D-π-A)[24–26] and octupolar structures ((D-π-A)3)[27–30], where D and A refer to the electron-donating and electron-withdrawing groups respectively, linked through a bridge of π-conjugated bonds. On the other, some authors also followed the oligomeric strategy and explored the possibility of designing organic molecules exhibiting at the same time a strong 2PA and a good transparency[31]. Recently, great efforts have been focused

on the synthesis of octupolar structures since they have demonstrated strong electronic coupling between the individual arms, giving rise to prodigious hyperpolarizabilities[27]. Moreover, as it has been shown by some of us[32,33], even for octupolar molecules whose permanent dipole moment vanishes in the gas phase, aggregation can still take place due to the thermal motions of atoms and strong intermolecular interactions.

Among the octupolar structures, push-pull triarylamine compounds stand out due to their good electrondonating and -transporting capability. Thereby, their noteworthy electronic and optical properties have been harnessed in different applications as active layers for two-photon holographic rewritable micropatterning[34], fluorescence photoswitching[35], or dye-sensitized solar cells[36]. However, for most of the triarylamine compounds reported so far, the overlap of the π molecular orbitals (MOs) carrying the nitrogen lone pair with the π MOs on the phenyl rings is relatively poor due to the large dihedral angle between the planes containing the phenyl ring on one side and the nitrogen-bonded carbon atoms on the other side[37], hence the 2PA performances were severely impaired. We want here to investigate the influence of the introduction in the positions 3 and 5 of the phenyl rings of electron-withdrawing groups such as the trifluoromethyl (CF3) one, and the distinct strength of the electron-withdrawing groups (**H** < **CN** < **CHO** < **NO2** < **Cyet** < **Vin**) upon the 2PA property of triarylamine derivatives. Furthermore, the CF_3 group imparts organic molecules with hydrophobic properties which exert positive influence on their use as biologically active compounds[38]. In this context, we reported here a comprehensive experimental and theoretical study on the 1PA and 2PA properties of six push-pull triarylamine molecules containing trifluoromethyl (CF_3) and distinct electron-withdrawing groups (EWG). Since these molecules present octupolar structures with phenyl bridges and strong electron-donating (triarylamine) and electron-accepting (trifluoromethyl) groups, large changes in dipole moment upon excitation are expected. Presumably, the presence of the CF_3 may result in enhanced charge transfer from the amino core toward the CF_3-biphenyl groups in one of the excited states. For the 2PA measurements, we employed the open-aperture Z-scan technique using an optical parametric amplified pumped by a femtosecond laser system operating at a low repetition rate (1 KHz). Two and three-energy level approximations helped us establish a quantitative relationship between the 2PA and the molecular properties of the chromophores in solution. This relationship is established by comparing the values of the transition dipole moments μ and dipole moment changes Δμ obtained from 2PA and solvatochromic shift measurements. The results were also compared with theoretical predictions of the one- and two-photon transitions strengths, transition dipole moments and dipole moment changes upon excitation, provided by response function calculations within the density functional theory (DFT) framework[39,40]. Linear optical properties such as molar absorptivity, one-photon induced fluorescence, transition and permanent dipole moments, fluorescence quantum yields and lifetimes also are reported.

Results

Synthesis of the push-pull triarylamine compounds. The synthesis of the targeted compounds proceeded via a Suzuki aromatic coupling reaction between the commercially available 3,5-bis(trifluoromethyl) phenylboronic acid and various bis(4-bromophenyl)phenylamino derivatives differing by the nature of their electron-withdrawing group (Figure 1). In this way, four derivatives **CF_3X** where X = H, CN, CHO and NO_2 could be obtained as white to bright yellow solids. The last two derivatives **CF_3Cyet** and **CF_3vin** were issued from an additional Knoevenagel reaction between **CF_3CHO** and ethyl cyanoacetate and malononitrile respectively, assisted by ammonium acetate as an acidic catalyst in a solvent mixture of pyridine:acetic acid (10 : 1). The compounds appear as bright orange-yellow solids. All six compounds were carefully purified by chromatography column before studies.

One-photon absorption and emission, oxidation potentials. The ground-state absorption and emission spectra of the push-pull triarylamine derivatives **CF_3EWG** are illustrated in Fig. 2a and 2b, respectively. All molecules present an intense absorption band in the UV range around 350–370 nm. A second absorption band appears at lower energy in the visible range for compounds **CF_3NO_2**, **CF_3Cyet** and **CF_3vin**. Interestingly, compared to their homologous derivatives **tBuEWG**, substituted by electron-donating *tert*-butyl groups the *para*-phenyl positionthe **CF_3EWG** series, substituted by two electron-withdrawing trifluoromethyl groups in the *meta* positions, exhibit bathochromic and hypsochromic shifts of their UV and visible

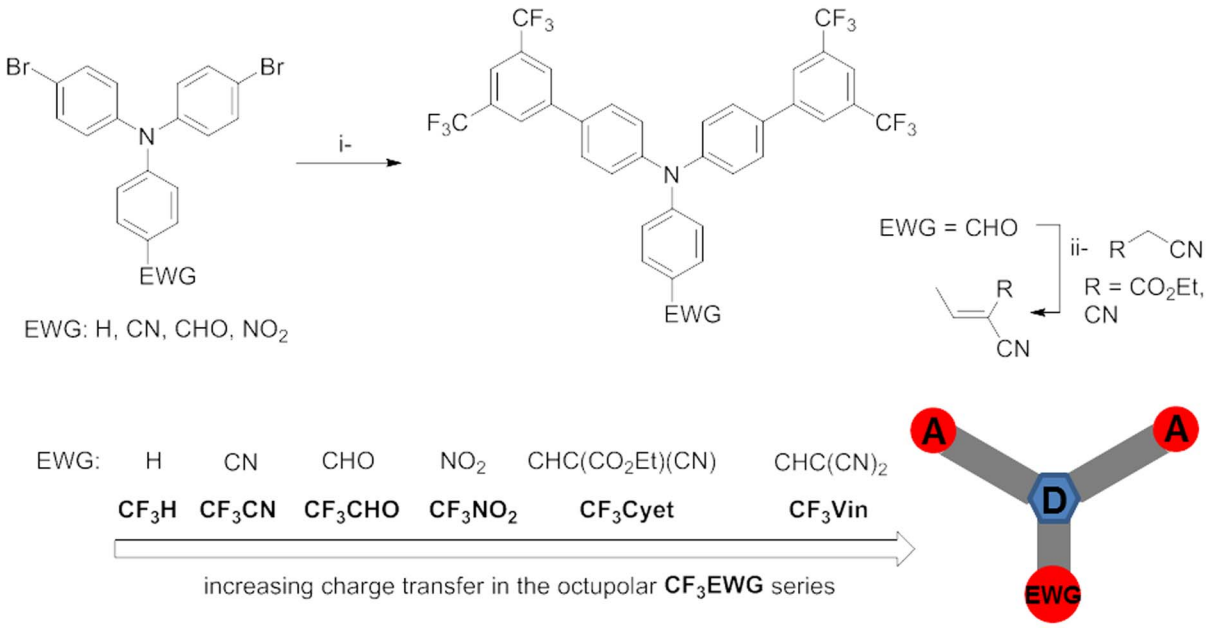

Figure 1 | Synthetic pathway toward the octupolar push-pull triarylamine compounds CF_3EWG: i- 3,5-bis(trifluoromethyl)phenylboronic acid, $Pd(PPh_3)_4$, Na_2CO_3 2 mol.L^{-1}, toluene, 80°C, 8 h; ii- ethyl cyanoacetate or malononitrile, pyridine:acetic acid (10 : 1), NH_4OAc, RT, 6 h.

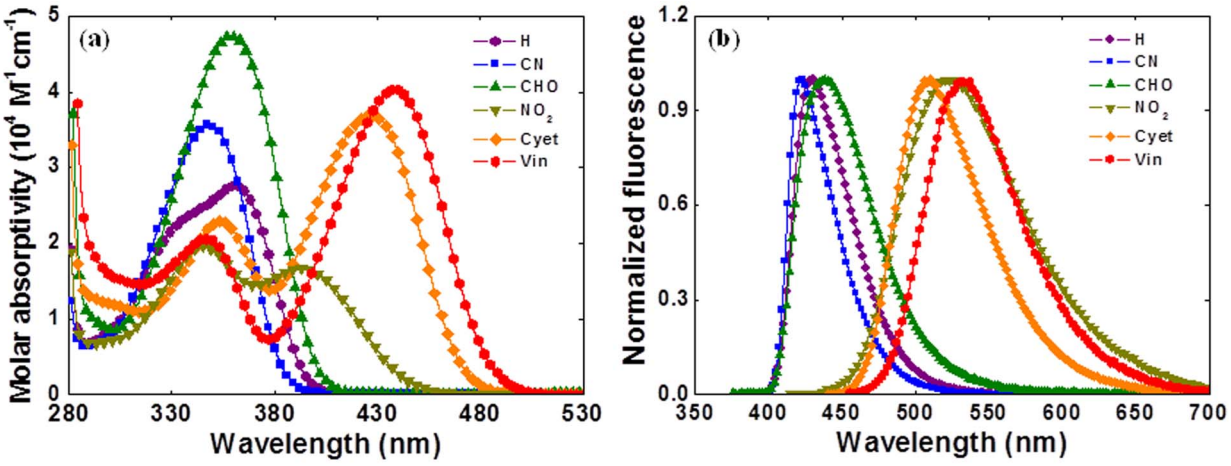

Figure 2 | (a) Ground-state absorption and (b) fluorescence spectra of push-pull triarylamine derivatives containing CF_3 in toluene solutions.

absorption bands respectively. However, their molar absorption coefficients ε are similar to those obtained for the **tBuEWG** series[41,42].

As for the absorption spectra, only one fluorescence band is observed in the visible region. Interestingly, two kinds of photophysical behaviors can be distinguished. The first one relates to compounds **CF_3NO_2**, **CF_3Cyet** and **CF_3vin**. All three display an emission band centered around 520 nm and a large Stokes shift ranging from 3900 to 6300 cm^{-1}. As already discussed for the **tBuEWG** series[43], femtosecond transient absorption spectroscopy measurements showed that the compounds underwent a significant nuclear rearrangement in the excited state after a charge transfer occurred from the triphenylamino core onto the EWG unit. The second behavior is described by compounds **CF_3H**, **CF_3CN** and **CF_3CHO** which exhibit an emission band centered around 430 nm and similar Stokes shifts ranging from 4300 to 5100 cm^{-1}. Compared to the other two compounds, the emission band of **CF_3CHO** lies at lower energy in accordance with the more red-shifted wavelength of the corresponding maximum absorption. Finally, the emission of **CF_3H** in toluene located at 428 nm instead of 383 nm for the **tBuH** homologue shows a clear participation of the trifluoromethyl groups in the radiative excited state and presumably in the Franck-Condon state also.

The electronic influence of the CF_3 groups is clearly apparent in the oxidation of the triphenylamino core into a triphenylammonium cation as featured by the first redox potential (Table 1). All triarylamine derivatives **CF_3EWG** examined in this study displayed a quasi-reversible process characterized by an averaged redox potential E° ranging from 0.63 to 0.87 V (*vs* Fc^+/Fc) depending on the EWG substituents). Compared to the series of electron-donating compounds **tBuEWG**, the E° values rise by 0.17 to 0.2 V. This considerable increase, being much more significant for **CF_3H**, is to be ascribed to the electron-deficient character of the CF_3 groups, thus decreasing considerably the electron density located on the triphenylamino core in the ground state. No simple correlation between the electrochemical measurements and the optical gaps could however be traced, which is due to the high sensitivity of the excited state on the solvent polarity as it will be discussed later.

Character of electronic transitions and solvatochromic measurements. In order to investigate the nature of the transitions observed along the 1PA spectra, we performed the analysis of response vectors to determine the largest one-electron orbital excitations. As it can be noted in Fig. 3, the lowest-energy transition for the **H** and **CN** derivatives is a $\pi \rightarrow \pi^*$ transition involving the two trifluoromethyl-phenyl arms (acceptor groups). For all other compounds, the lowest-energy transition is an ICT transition involving the triarylamine core and the respective EWG. The reason of this ordering difference stems in the low strength of the **CN** substituent, which therefore does not promote the inversion between the π^* and ICT excited states as observed for all the other substituents. The influence of the EWG strength on this inversion is also evidenced by the

Table 1 | UV-vis absorption and emission properties in toluene solution

	H	CN	CHO	NO_2	Cyet	Vin
λ_{max}^{abs} (nm)	361	347	359	394	426	439
ε_{max} ($M^{-1}cm^{-1}$)	27550	35600	35600	16800	36900	40300
λ_{max}^{em} (nm)	428	422	437	525	510	535
ϕ_{max}^{em}[a] (nm)	0.46	0.24	0.19	0.40	0.13	0.24
τ_f[b] (ns)	2.2	2.7	2.1 (56%) 0.9 (44%)	3.5	0.85	1.0
E° (V) (ΔE_P mV)[c]	0.63	0.81	0.79	0.87	0.78	0.83
$\lvert\vec{\mu}_{00}\rvert^{exp}(D)$	1.1	1.6	1.25	2.4	3.3	3.6
$\lvert\vec{\mu}_{01}\rvert^{exp}(D)$	5.8	6.2	7.4	5.2	8.2	8.4
$\lvert\vec{\mu}_{02}\rvert^{exp}(D)$	4.9	5.5	6.0	5.5	6.4	6.0
$\lvert\vec{\mu}_{12}\rvert^{exp}(D)$	7.5	1.5	1.3	3.0	2.5	3.0
$\partial\upsilon/\partial F(cm^{-1})$	3240	2340	2420	3930	5150	5220
$Vol(\AA^3)$	751.48	783.02	782.73	789.32	915.81	873.63
$\lvert\Delta\vec{\mu}_{01}\rvert^{SS}(D)$	10.6	9.2	9.5	12.0	14.7	14.8
r	5.313	5.653	5.699	5.662	5.693	5.716
$r_{eff} = \lvert\Delta\mu\rvert/e$	2.20	1.92	1.98	2.60	3.06	3.08
$\bar{r}_{eff}/r$	42%	34%	35%	46%	54%	54%

[a] Fluorescence standard POPOP $\Phi = 0.93$ in cyclohexane. [b] $\lambda_{exc} = 349$ nm. [c] Measured in dichloromethane *vs* Fc^+/Fc with E° (Fc^+/Fc) = 0.178 V *vs* Ag/$AgNO_3$ used as a reference electrode. Obs: r is the distance between the core and the first EWG atom obtained from the DFT calculations, $r_{eff} = \lvert\Delta\mu\rvert/e$ defines the effective charge transfer, where e is the electron charge. $\bar{r}_{eff}/r$ is the degree of intramolecular charge transfer.

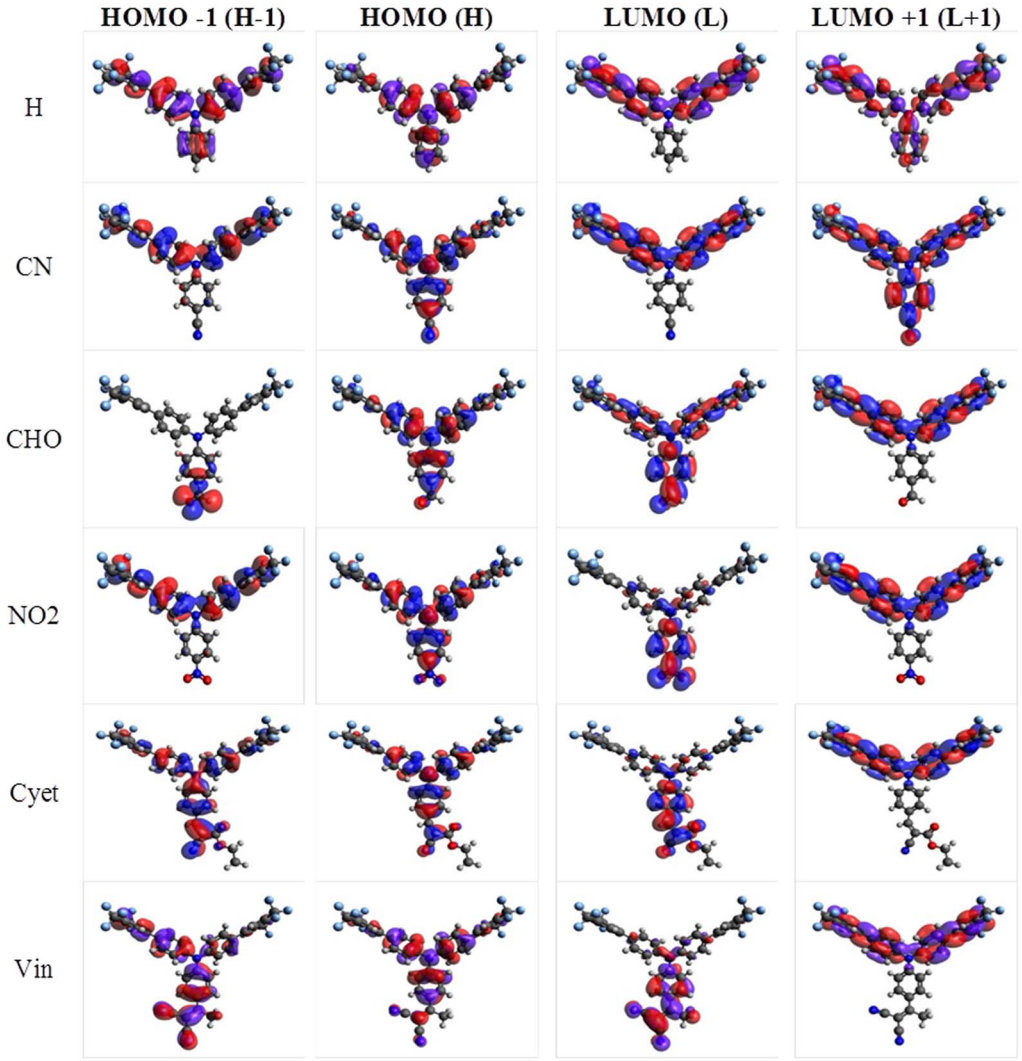

Figure 3 | KS molecular orbitals involved in the lowest–energy electronic transitions of the investigated molecules.

molecular orbital involved in the excitations of the **CHO** substituent. Because of its moderate EWG strength, the charge transfer from the triarylamine core to the EWG in the case of **CHO** substituent is not as pronounced as for the **NO_2**, **Cyet** and **Vin** substituents.

To shed more light on the character of electronic transitions, we performed solvatochromic Stokes shift measurements to find the difference between the permanent dipole moments in the excited and ground states, $\Delta\vec{\mu}_{01}^{SS}$. For this purpose, we used the Lippert-Mataga equation[44]:

$$\left|\Delta\vec{\mu}_{01}^{SS}\right|^2 = \frac{3\pi hc}{4}\frac{\partial\upsilon}{\partial F}Vol, \qquad (1)$$

where $\upsilon=\upsilon_A-\upsilon_{em}$ is the difference between the wavenumbers of the maximum absorption and fluorescence emission (in cm^{-1}), $F(n,\xi)=2(\xi-1)/(2\xi+1)-2(n^2-1)/(2n^2+1)$ is the Onsager polarity function with ξ being the dielectric constant of the solvent, Vol is the volume of the effective spherical cavity occupied by the molecule inside the dielectric medium. Various solvents or mixtures of solvents (cyclohexane, hexane, toluene, hexane/chloroform (50/50%), hexane/dichloromethane (50/50%), chloroform, dichloromethane, acetone and ethanol) with increasing polarity were investigated for all compounds.

A pronounced increase of the Stokes shift was found with increasing solvent polarity and reveals clearly the polar character of the radiative excited state (S_1) (Fig. 4). These results indicate that the absolute values of the excited state dipole moments $\vec{\mu}_{11}$ are much higher than those of the ground state dipole moments $\vec{\mu}_{00}$.

From the Fig. 4, we found $\frac{\partial\upsilon_H}{\partial F}=3280\pm370cm^{-1}$, $\frac{\partial\upsilon_{CN}}{\partial F}=2340\pm165cm^{-1}$, $\frac{\partial\upsilon_{CHO}}{\partial F}=2420\pm160cm^{-1}$, $\frac{\partial\upsilon_{NO_2}}{\partial F}=3930\pm350cm^{-1}$, $\frac{\partial\upsilon_{Cyet}}{\partial F}=5150\pm510cm^{-1}$ and $\frac{\partial\upsilon_{Vin}}{\partial F}=5220\pm780cm^{-1}$. Using these data, the hydrodynamics volume estimated from the IEF-PCM/B3LYP/6311G(d,p) calculations (see Table 1) and the Eq. 3, we found $\left|\Delta\vec{\mu}_{01}^{H}\right|=10.6D$, $\left|\Delta\vec{\mu}_{01}^{CN}\right|=9.2D$, $\left|\Delta\vec{\mu}_{01}^{CHO}\right|=9.5D$, $\left|\Delta\vec{\mu}_{01}^{NO_2}\right|=12.5D$, $\left|\Delta\vec{\mu}_{01}^{Cyet}\right|=14.7D$ and $\left|\Delta\vec{\mu}_{01}^{Vin}\right|=14.8D$. These results show that all molecules present pronounced $\Delta\mu_{01}$ values (between 9 to 15 Debye) indicating a high degree of effective charge transfer (>34%), which can be obtained from the relation $r_{eff}=|\Delta\mu|/e$, where e is the electron charge[45]. Table 1 reports the degree of charge transfer observed for all molecules.

As one can note, the degree of ICT ($\bar{r}_{eff}/r$), where r is the distance between the core and the first EWG atom obtained from the DFT calculations, for the molecules **CF_3CN** and **CF_3CHO** is considerably smaller than that of **CF_3H**, even though the cyano and aldehyde substituents have a higher EWG strength. Another important outcome that we can infer from these results is the increase in the degree

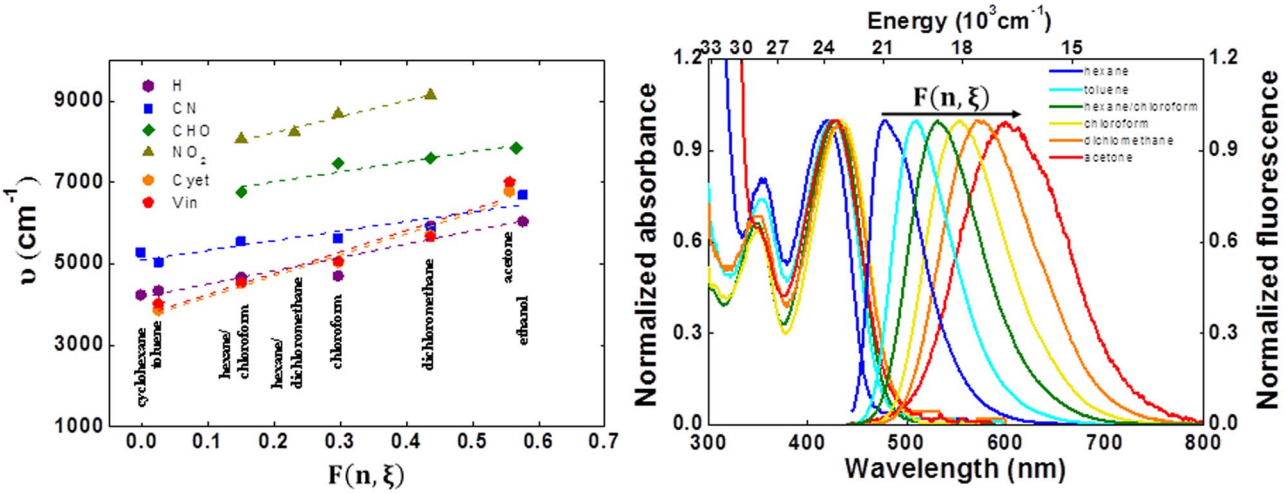

Figure 4 | (a) Solvatochromic Stokes shift (υ) measurements obtained as a function of the Onsager polarity function ($F(n, \xi)$) for all molecules in a series of different solvents (cyclohexane, hexane, toluene, hexane/chloroform, chloroform, dichloromethane, acetone and ethanol). (b) Solvatochromic measurements for **CF_3Cyet** molecule illustrating the increase of the Stokes shift with the increase of the solvent polarity for this class of molecules.

of ICT caused by higher splitting of the lowest energy 1PA band. The splitting in quasi-degenerate excited states is a result of the interactions between the arms of the chromophores[27]. Whereas no such splitting could be experimentally distinguished for **CF_3CN** and **CF_3CHO** that have the lowest values of ICT, clear interactions could be noticed for the other four compounds: a shoulder on the lowest energy band for **CF_3H** with an energetic separation of ~300 meV, and a considerable splitting for **CF_3NO_2** (~460 meV), **CF_3Cyet** (~610 meV) and **CF_3Vin** (~740 meV). We used the Gaussian decomposition method to estimate the splitting energy for **CF_3CN** and **CF_3CHO** and obtained 240 meV and 250 meV, respectively. From these values and based on the exciton Frenkel model[27], we estimated the electronic coupling constant for all octupolar structures as being ~100 meV for **CF_3H**, ~80 meV for **CF_3CN** and **CF_3CHO**, ~155 meV for **CF_3NO_2**, ~205 meV for **CF_3Cyet** and ~245 meV for the **CF_3Vin**. As a conclusive point, our results show that the electronic coupling is directly proportional to the degree of ICT of EWG.

Table 1 also reports the photophysical parameters of push-pull triarylamine derivatives containing CF_3, such as: maximum absorption and fluorescence wavelengths, maximum molar absorptivity, experimental ground-state ($|\vec{\mu}_{00}|$) and transition dipole moment ($|\vec{\mu}_{01}|$), fluorescence quantum yield and lifetime determined in this work by using a series of spectroscopic techniques. All molecules show a significant fluorescence quantum yield with average lifetimes of the order of 2 ns.

Experimental 2PA properties. Figure 5 shows the experimental 2PA spectra (dots) determined by performing open-aperture Z-scan measurements with femtosecond pulses. The experimental data reveal well-defined 2PA spectra with moderate cross-section values (from several tens to few hundreds of GM units) in the visible and infrared regions depending on the electronic influence of the withdrawing substituents.

Along the 2PA spectra we can distinguish, except the molecules with the lowest degree of ICT (**CF_3CN** and **CF_3CHO**), three 2PA allowed bands and the resonance enhancement effect[46,47]. Among the three 2PA bands, those two ones of lower energy are related to the ICT ($S_0 \rightarrow S_1$) transition and the π-π^* ($S_0 \rightarrow S_2$) transition located on the trifluoromethyl-phenyl arms in agreement with the linear absorption spectra. This assumption is supported by the good spectral correspondence observed between the bands in the 2PA and 1PA spectra (see Fig. 5) and also by the results of the response function calculations (see theoretical results section). Slight blue shifts between the spectral position of 1PA and 2PA peaks may be ascribed to the distinct vibronic coupling between the ground- and excited-states in the 1PA and 2PA transitions. Although the computational strategies to include vibronic coupling are well established[48], we have not attempted to apply them in the present study. The primary reason is that the experimental 2PA spectra do not exhibit a fine vibrational structure for the absorption bands. However, in the case of multi-branched structures, vibronic contributions to the two-photon absorption may be substantial[48]. It is important to mention that two-photon transitions are different from the one-photon ones and, moreover, very strict. However, in compounds that present a low molecular symmetry, so that it is not possible to define the parity of excited states precisely, the same electronic state may be accessed via both one and two-photon absorptions[49].

It is worth mentioning that, for all molecules, the highest energy 2PA band has the highest cross-section values that are between 95 GM (for **CF_3H**) to 270 GM (for **CF_3Vin**). This band is associated with electronic states that present high 2PA probability located in the UV region (from 260 nm to 300 nm).

The cross-section values, at the peak of the main 2PA bands, were determined to be *c.a.*65 GM at 725 nm, 83 GM at 620 nm and 97 GM at 520 nm for **CF_3H**; 58 GM at 715 nm and 145 GM at 560 nm for **CF_3CN**; 48 GM at 720 nm and 262 GM at 580 nm for **CF_3CHO**; 45 GM at 800 nm, 58 GM at 680 nm and 230 GM at 585 nm for **CF_3NO_2**; 115 GM at 850 nm, 68 GM at 700 nm and 250 GM at 610 nm for **CF_3Cyet**; 125 GM at 880 nm; 70 GM at 700 nm and 265 GM at 605 nm for **CF_3Vin**. The 2PA cross-section values reported here for the triarylamine molecules containing CF_3 are at least 30% higher than those reported for their *tert*-butyl analogues[41,42]. However, we cannot attribute this 2PA enhancement to the CF_3 groups because this difference may be associated only with the higher polarity of solvent used in this present report (toluene) when compared to the results of Refs[40,41]. (hexane). To overcome this doubt, we performed 2PA measurements using the Z-scan technique for the *tert*-butyl analogues in toluene solution and, in fact, observed 2PA cross-section values similar ones reported here to the molecules containing CF_3 groups.

Analogously to what was found in the 1PA spectra of **CF_3CN** and **CF_3CHO**, no splitting between the two lowest energy 2PA transitions is observed along the nonlinear spectra. Additionally, the peak of lowest energy 2PA band is slightly red-shifted (50 meV) as compared to the corresponding 1PA peak, indicating that the $S_0 \rightarrow S_1$

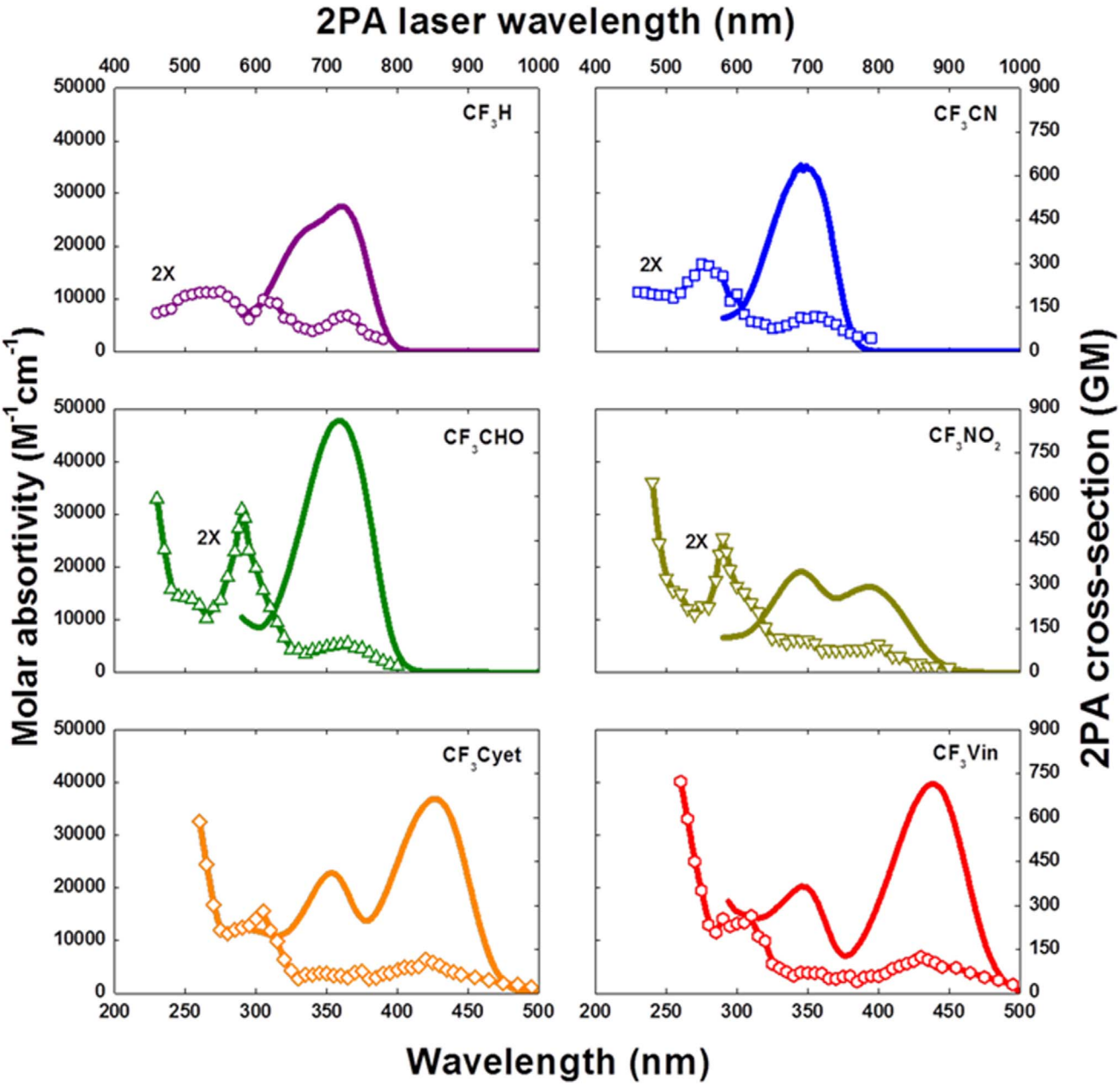

Figure 5 | The solid lines and dots represent, respectively, the linear and two-photon absorption spectra. 2PA cross-sections for the CF_3H, CF_3CN, CF_3CHO and CF_3NO_2 molecules were multiplied by 2 for better comparison with the others molecules.

transition dominate the nonlinear optical effect in this region. This result can be attributed to the low electronic coupling constant observed for these molecules (~80 meV).

For the other molecules, as it was observed in the 1PA spectra, the 2PA spectra exhibit a clear and increasing (in energy) splitting of the lowest energy band as a function of increase of the degree of ICT. Our results point out that for **CF_3H** ($\sigma^{S2}_{2PA}/\sigma^{S1}_{2PA} = 1.3$) and **$CF_3NO_2$** ($\sigma^{S2}_{2PA}/\sigma^{S1}_{2PA} = 1.2$), the π-π^* ($S_0 \rightarrow S_2$) transition has higher 2PA cross-section values than that of the corresponding $S_0 \rightarrow S_1$ transition, whereas for **CF_3Cyet** ($\sigma^{S2}_{2PA}/\sigma^{S1}_{2PA} = 0.59$) and **$CF_3$Vin** ($\sigma^{S2}_{2PA}/\sigma^{S1}_{2PA} = 0.56$) the opposite is found. This result can be at least partially explained due to the lower transition dipole moment ($|\vec{\mu}_{01}|$), observed for **CF_3H** and **CF_3NO_2** as compared to **CF_3Cyet** and **CF_3Vin**. In the context of the sum-over essential states approach, the 2PA cross-section of the lowest energy transition, which is proportional to the product of $|\vec{\mu}_{01}|^2$and $|\Delta\vec{\mu}_{01}|^2$, became less intense.

Since the 2PA cross-section of the $S_0 \rightarrow S_2$ transition for **CF_3H** is the highest one despite a larger ICT encountered for the other octupolar compounds **CF_3NO_2**, **CF_3Cyet** and **CF_3Vin**, one can suspect for **CF_3H** a large electronic coupling between its bis(trifluoromethyl)biphenyl arms upon 2PA excitation. The lower 2PA cross-sections for **CF_3NO_2**, **CF_3Cyet** and **CF_3Vin** molecules may be due to increased angular torsions of the **NO_2**, **Cyet** and **Vin** substituents around the phenyl-N bonds, thus leading to a reduced electronic coupling between the arms and, as a consequence, a decrease in the 2PA cross-section of $S_0 \rightarrow S_2$ electronic transitions.

To establish a more quantitative relationship between the effect of distinct EWG and the observed 2PA activity, we used the sum-over-essential states approach to determine the permanent dipole moment change between the ground and excited states and the transition dipole moments between excited states. Details about this approach can be found in "Supporting information". Figure 6 shows a comparison between the $|\Delta\vec{\mu}^{2PA}_{01}|$ values obtained from 2PA and

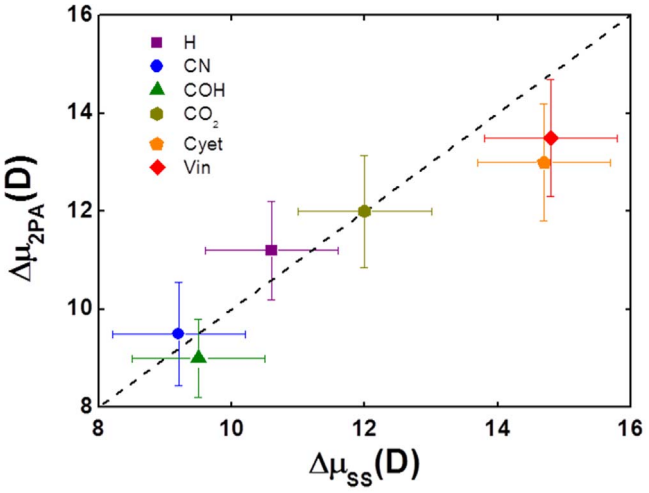

Figure 6 | Comparison of the permanent dipole moment change ($\Delta\vec{\mu}_{01}$) obtained from 2PA and solvatochromic Stokes shift measurements.

solvatochromic shift measurements. As it can be observed in Fig. 6, there is a good agreement between the results determined from 2PA and **solvatochromic shift** measurements. These results show that the lowest-energy 2PA band for all molecules can be well-described by a two-level system.

To model the $S_0 \rightarrow S_2$ 2PA allowed transition, we considered a three-level system composed of the ground state (S_0), one intermediate 1PA allowed excited state ($|1\rangle$) and the 2PA allowed final excited state (S_2). Table 1 shows the results obtained using the methodology described in "Supporting information". The main aspect to be highlighted, based on these results, is that upon going from the neutral substituent (H) to the strongest EWG (Vin), the transition dipole moment that connects the two lowest energy 2PA allowed states, $|\vec{\mu}_{12}|$, decreases by about 2.5–5 times, due to the influence of the EWG on the electronic coupling between the arms of the octupolar structure. For CF_3CN and CF_3CHO, a decrease in the transition dipole moment $|\vec{\mu}_{12}|$ was expected since these molecules present lower electronic coupling constant as compared to CF_3H. For the other molecules, the NO_2, Cyet and Vin substituents should increase the angular torsion of the whole plane phenyl-EWG along the N-phenyl bond, which impairs electronic coupling between the arms, thus decreasing $|\vec{\mu}_{12}|$. In this context, the structure–property relationships outlined in this study are of foremost importance for the development of novel organic materials with remarkable nonlinear optical properties.

Theoretical results. In what follows, we present the results of quantum-chemical calculations of the electronic structures of triarylamine molecules using response functions. The data presented in Table 2 correspond to the results of calculations performed using reparametrized CAM-B3LYP functional and some additional information extracted from the experimental data. In general, a satisfactory agreement between the transition energies determined by the response function calculations and through the theoretical fitting of the experimental 1PA spectrum is observed. The difference found for the lowest energy transition $S_0 \rightarrow S_1$ is smaller than 0.15 eV for all molecules. In the case of the second transition reported in Table 2, $S_0 \rightarrow S_{n=2,3}$, the difference observed is smaller than 0.18 eV basically for all molecules, the only exception (0.26 eV) being the case of CN substituent.

The states accessed via two-photon transitions are also allowed via one-photon transition as shown by the reasonable oscillator strength obtained for all the transitions (see Table 2). Such results confirm that the electric-dipole selection rules are relaxed for all the compounds investigated, which was expected due to the absence of centrosymmetric.

By comparing the results of the gas-phase (not shown) and PCM calculations, the solvent effects promote a red-shift and the increase in the oscillator strength for all transitions, the only exception being the second transition of **Cyet** substituent that shows a small blue-shift. In addition, the comparison shows that the solvent effects promote a 2PA probability increase for all the transitions of the investigated substituents. The solvent effects increase the 2PA probability by about 80–130%. To better compare the experimental data and theoretical results for 2PA process, we simulated the 2PA cross-section spectrum of the triarylamine molecules by using the excited state linewidths estimated by fitting the experimental linear spectra and the 2PA transition probabilities determined by the quadratic response calculations (see Table 2). The simulated and experimental 2PA cross-section spectra are presented in Figure 7. As it can be seen, there is a good agreement between the simulated and experimental spectra both for the spectral behavior and cross-section magnitude.

For each investigated molecule, the simulated 2PA cross-section spectrum reproduces the bands observed over the experimental spectrum. The magnitude of the 2PA cross-section at the peak of each absorption band observed in the experimental spectrum and the related value in the simulated spectrum are gathered in Table 2.

Discussion

The experimental 2PA cross-sections observed along the nonlinear optical spectra for the **CF_3EWG** molecules as a function of the nature of the electron-withdrawing group can be explained from the competition among the EWG strength, the degree of donor-acceptor charge transfer and the electronic coupling among the arms present in each molecule. Based on these parameters, our experimental results showed that the **Cyet** and **Vin** substituents favors the first 2PA band (which has the ICT character) in detriment to their second band due to the poor electronic coupling between the arms and the strong donor-acceptor (N→EWG) charge transfer. However, **CF_3Cyet** and **CF_3Vin** have an electronic coupling constant higher than those observed in the case of **CF_3H** and **CF_3NO_2** which present 2PA cross-sections higher to the second 2PA band as compared with the first one. Nevertheless, in solution, the octupolar **CF_3Cyet** and **CF_3Vin** molecules present a considerable increase in angular torsions of the whole plane phenyl-EWG along the N-phenyl bond that lead to a reduced electronic coupling between the arms, thus decreasing the 2PA cross-section of the $S_0 \rightarrow S_2$ electronic transition. These angular torsions were recently observed through femtosecond transient absorption spectroscopy measurements for similar molecules. On the other hand, for **CF_3CN** and **CF_3COH**, the fact of the $S_0 \rightarrow S_1$ transition dominates the lowest energy 2PA band (at least 70%) is due exclusively to the low electronic coupling constant observed for these molecules (~80 meV).

All **CF_3EWG** molecules present the highest energy 2PA band with the highest cross-section value which ranges from 95 GM for **CF_3H** to 270 GM for **CF_3Vin**. This band is associated with an cluster of electronic transitions that present high 2PA probability located in the UV region (from 260 nm to 300 nm) as well as the resonance enhancement effect due to the little detuning between the excitation energy and the energy of the lowest energy one-photon allowed state.

By comparing the magnitude of the 2PA cross-section of the two lowest energy transitions, the theoretical results and experimental data show a nice match, *i.e.* in the case of the **H** and **NO_2** substituents the higher energy transition presents a larger cross-section. For the remaining substituents, the theoretical results and experimental data do not agree about which transition presents the higher 2PA cross-section. At least two factors may dramatically affect the agreement between the theoretical results and experimental data. In the case of the **CN** and **CHO** substituents the two-lowest energy transitions are close in energy, as evidenced by the theoretical results and

Table 2 | Experimental data and theoretical results of the PCM/Reparametrized-CAMB3LYP calculations using the linear and quadratic response functions. Transition energies (E) in nm, oscillator strength, two-photon transition probability (P) in a.u., dipole moment changes ($\Delta\mu$) in Debye and two-photon absorption cross-section (σ) in GM. The molecular orbitals involved in the excitations describing the electronic transitions reported are also showed. $|\Delta\vec{\mu}_{0i}^{\exp}|$ is one obtained from the 2PA cross-section data

	E_{0i}^{theo}	$E_{0i}^{\exp}$	f_{0i}^{theo}	$f_{0i}^{\exp}$	P	Excitations	$\lvert\Delta\vec{\mu}_{0i}^{theo}\rvert$	$\lvert\Delta\vec{\mu}_{0i}^{\exp}\rvert$	$\sigma_{0i}^{(theo)}$	$\sigma_{0i}^{(\exp)}$
	370 (S_1)	363	0.89 (3.29D)	0.44 (5.8 D)	10400	H→L (89%)	5.96	10.5	45	65
H	337 (S_3)	337	0.43 (2.17 D)	0.34 (4.9 D)	36700	H→L+1 (74%)	0.08	2.0	98	83
	280 (S_8)	NA	0.000 (0D)	NA	75200				285	97
	361 (S_1)	353	0.73 (2.93D)	0.52 (6.2 D)	9140	H→L (87%)	3.86	9.5	20	58
CN	354 (S_2)	330	0.73 (2.63D)	0.44 (5.5 D)	13300	H→L+1 (89%)	7.47	6.7	67	14[a]
	280 (S_8)	NA	0.000 (0D)	NA	92800				362	145
	381 (S_1)	365	0.74 (3.04D)	0.67 (7.4 D)	11200	H→L (93%)	6.66	9.0	36	48
CHO	356 (S_2)	339	0.73 (2.93D)	0.51 (6.0 D)	14900	H→L+1 (89%)	7.71	4.5	43	15[b]
	290 (S_7)	NA	0.005 (0.23D)	NA	107000				405	262
	416 (S_1)	395	0.67 (3.03D)	0.32 (5.1 D)	26900	H→L (92%)	10.53	11.5	57	45
NO_2	352 (S_2)	344	0.69 (2.80D)	0.41 (5.5D)	14700	H→L+1 (87%)	7.56	8.6	78	58
	299 (S_5)	NA	0.065 (0.80D)	NA	102000				335	230
	424 (S_1)	426	1.05 (4.13D)	0.75 (8.2 D)	39900	H→L (94%)	9.30	13.0	79	115
Cyet	348 (S_2)	352	0.54 (2.61D)	0.55 (6.4 D)	22900	H→L+1 (84%)	9.90	7.5	109	68
	298 (S_5)	NA	0.007 (0.31D)	NA	134000				445	265
	430 (S_1)	437	0.85 (3.55D)	0.78 (8.4 D)	45600	H→L (92%)	11.53	13.5	85	125
Vin	352 (S_2)	348	0.65 (2.74D)	0.50 (6.0 D)	20700	H→L+1 (85%)	8.84	8.0	104	70
	306 (S_4)	NA	0.056 (0.86D)	NA	122000				381	270

Obs: a and b represents the 2PA cross-section values estimated for the $S_0 \rightarrow S_2$ transition using the sum-over-essential states approach.

the structureless band observed in their 1PA spectrum. In such a situation, the accuracy of the procedure to fit the experimental linear spectra and estimate the spectral linewidth of the related excited states, which is then used to compute the 2PA cross-sections, cannot be completely reliable. Since for the **CN** and **CHO** substituents, the 2PA transition probability of the two lowest energy transitions are roughly similar, an accurate estimative of the linewidth of the excited states is crucial to determine which transition presents the higher 2PA cross-section. For the **Cyet** and **Vin** substituents, on the other hand, the two-lowest energy transitions are separated in energy and, therefore, the estimated values of the spectral linewidths are more reliable. Also, the 2PA probabilities of the two lowest energy transitions are quite different for these substituents. In order to find a plausible explanation for these differences, the electronic character of the lowest-energy transitions should be further investigated.

A good agreement between theoretical results and experimental data concerning the efficiency of the distinct EWG in increasing the 2PA cross-section of the $S_0 \rightarrow S_1$ transition is observed. For the **CHO**, **NO_2**, **Cyet** and **Vin** substituents, the cross-section ordering basically agrees with the EWG strength ordering (**CHO** < **NO_2** <**Cyet**< **Vin**). As mentioned above, in the case of **CN** substituent, such a transition does not involve its EWG. The quantitative agreement between theoretical and experimental 2PA cross-section is, however, satisfactory.

Because the second-lowest energy transition of the **CHO**, **NO_2**, **Cyet** and **Vin** substituents is a $\pi \rightarrow \pi^*$ transition centered on the two trifluoromethyl-phenyl arms of these systems, the 2PA cross-section of such transitions is expected to be enhanced by the coupling between the arms. In addition, since trifluoromethyl is an EWG, in principle its presence also contributes to the intensity of the 2PA transition centered on the arms. The higher theoretical values for the 2PA cross-section of the $\pi \rightarrow \pi^*$ transition in comparison with the experimental values for such substituents may feature an impaired coupling due to the mobility of the arms in solution. Moreover, by comparing the present results for the **CHO**, **NO_2** and **Vin** substituents with the results of a previous study in which similar systems without trifluoromethyl groups were investigated[42], one can conclude that effects of the presence of the trifluoromethyl group are not significant for the 2PA transition. In fact, by checking the electron density distribution of the molecular orbitals (Figure 7) involved in the excitation describing the $\pi \rightarrow \pi^*$ transition, one can observe that the trifluoromethyl groups do not take part in such a transition.

Methods

Compounds. All chemical reagents and solvents were purchased from commercial sources (Aldrich, Acros, SDS) and used as received. Spectroscopic grade solvents purchased from Aldrich were used for spectroscopic measurements. Bis(4-bromophenyl)phenylamine[42], 4-di(4-bromophenyl)aminobenzonitrile[42], 4-di(4-bromophenyl)aminobenzaldehyde[42] and bis(4-bromophenyl)-4-nitrophenylamine[34] were synthesized according to previous reported procedures. Details about the synthesis for the **CF_3H, CF_3CN, CF_3COH, CF_3NO_2, CF_3Cyet, CF_3Vin** molecules can be found in "Supporting information".

Electrochemical measurements. Electrochemical measurements were performed with a three-electrode cell consisted of a glassy carbon working electrode (1.5 mm diameter), a counter electrode made of a Pt wire coil and an Ag/Ag+ reference electrode. The Ag/Ag^+ reference electrode was obtained by introducing a silver wire in the reference compartment containing silver ions ($AgNO_3$, 0.01M) and tetrabutylammonium perchlorate (TBAP, 0.1 M) in acetonitrile. The measured redox potential were expressed *vs* ferrocene used herein as internal reference. The triarylamine solutions were prepared in dichloromethane solvent added with 0.1 M of tetrabutylammonium hexafluorophosphate (Bu_4NPF_6) as a supporting electrolyte (Sigma-Aldrich). The solutions were deoxygenated by argon bubbling prior to each experiment. Cyclic voltammograms (CVs) were performed with VSP potentiostat controlled by EC-Lab 10.02 software. Both potentiostat and software were purchased from Bio-Logic Instruments-France.

1PA and 2PA measurements. Triarylamine derivatives/toluene solutions were prepared with concentrations of 1×10^{16} molecules/cm^3 and on order of 10^{18} molecules/c-m^3 for linear and nonlinear optical measurements, respectively. The samples were placed in 2 mm thick quartz cuvettes for optical measurements. The steady-state absorption and photoluminescence spectra were recorded using a Shimadzu UV-1800 spectrophotometer and a Perkin Elmer LS55 fluorimeter, respectively.

The nonlinear optical properties were measured by using, the open aperture Z-scan technique, employing 120-fs laser pulses from an optical parametric amplifier pumped by 150-fs pulses (775 nm) from a Ti:sapphire chirped pulse amplified system. The Z-scan measurements were carried out with intensities ranging from 60 to 200 GW/cm^2 (30 to 120 nJ/pulse) and with beam waist size at the focus varying from 15 to 18 μm. To ensure a Gaussian profile for the laser beam used in the experiments, spatial filtering is performed before the Z-scan setup. A silicon detector was employed to monitor the laser beam intensity in the far-field. To improve the signal to noise ratio, the oscillatory Z-scan method was used such that the samples are continuously scanned, repeating the experiment several times.

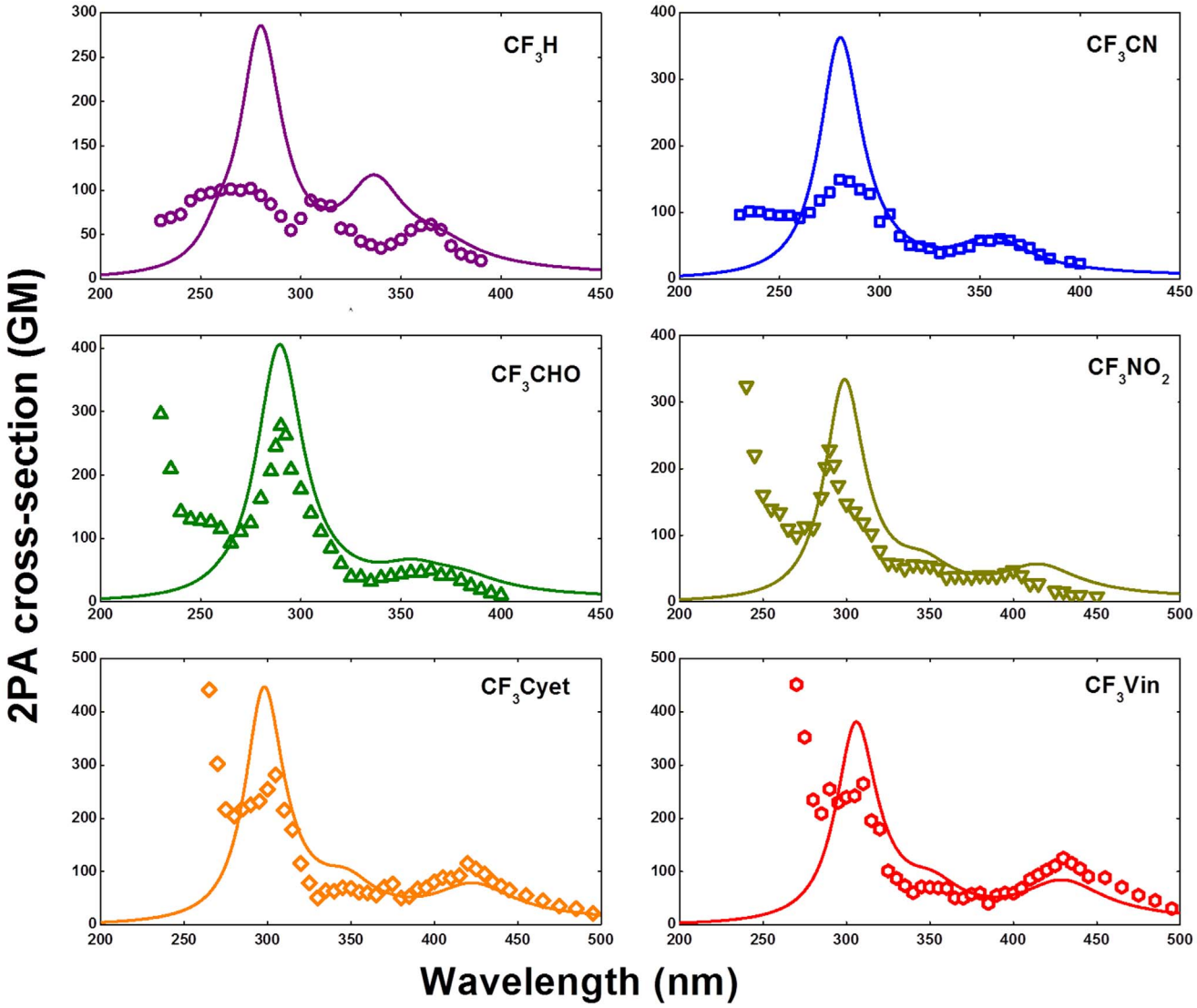

Figure 7 | The dots represent the experimental 2PA cross-section spectra. The solid lines correspond to the simulated 2PA cross-section spectra obtained using the 2PA transition probabilities determined by the response function calculations and excited states linewidths estimated by fitting the experimental nonlinear spectra using the sum-over essential states approach.

Moreover, a lock-in amplifier served to integrate 1000 shots for each point of the Z-scan signature.

In the open aperture *Z*-scan technique, 2PA cross-section was determined by translating the sample through the focal plane of a focused Gaussian beam, while transmittance changes in the far field intensity are monitored. For a 2PA process, the light field created an intensity dependent absorption, $\alpha = \alpha_0 + \beta I$; in which I is the laser beam intensity, α_0 is the linear absorption coefficient, and β is the 2PA coefficient. The nonlinear coefficient β was obtained by fitting the *Z*-scan data. The 2PA cross-section, σ_{2PA}, was determined from $\sigma_{2PA}=\hbar\omega\beta/N$, where $\hbar\omega$is the excitation photon energy, and N is the number of chromophores per cm^3. The 2PA cross-section was expressed in Göppert-Mayer (GM) units, where $1GM=1\times10^{-50}cm^4.s.photon^{-1}$.

Fluorescence quantum yield and time resolved measurements. Steady-state emission spectra were recorded using a Perkin Elmer LS55 or a Fluoromax 3 (Horiba-Jobin-Yvon) spectrofluorimeters respectively. Fluorescence intensity decays were measured by the time-correlated single-photon counting method (TCSPC) with a femtosecond laser excitation at 340 or 400 nm provided by a Spectra-Physics setup composed of a Titanium-Sapphire Tsunami laser pumped by a doubled YAG laser (Millennia), pumped itself by a two-laser diode array, and doubling and tripling LBO crystals. Light pulses were selected by optoacoustic crystals at a repetition rate of 4 MHz. Fluorescence photons were detected at the emission maximum through a monochromator by means of a Hamamatsu MCP R3809U photomultiplier, connected to a constant-fraction discriminator. The time-to-amplitude converter was from Tennelec. Pulse deconvolution was performed from the time profile of the exciting pulse recorded under the same conditions by using a Ludox solution. The fluorescence data were analyzed by a nonlinear least-squares global method using the Globals software package developed at the Laboratory for Fluorescence Dynamics at the University of Illinois at Urbana-Champaign (Globals software, Irvine, CA, USA).

Computational details. In this paper, quantum chemical calculations were employed to investigate the molecular and electronic structures of triarylamine molecules containing trifluoromethyl and determine their one-photon and two-photon transitions and related electronic structure parameters. For this purpose, quantum chemical calculations using the Kohn-Sham formulation of density functional theory (KS-DFT) were performed. The equilibrium molecular geometry of the molecules was determined in both gas-phase and solvent environment. The solvation effects on the equilibrium molecular geometry, the electronic structure and the one-photon and two-photon properties of each investigated molecule were taken into account by employing a Polarizable Continuum Model (PCM) and assuming the toluene solvent.

The gas-phase geometry optimizations were performed employing the B3LYP/6-311G(d,p) approach[50–52]. In the case of the geometry optimization taking into account the solvent environment, the PCM using the integral equation formalism variant (IEF-PCM)[10] was employed in combination with the B3LYP/6-311G(d,p) approach. All the geometry optimizations were performed using the Gaussian 2009 package[53]. The IEF-PCM method was combined with the United Atom for Hartree-Fock (UAHF) model to build the solute cavity. In this model the van der Waals surface is constructed from spheres located on heavy (that is, non-hydrogen) atoms only (United Atom approach). The van der Waals radius of each atom is a function of atom type, connectivity, total charge of the molecule and the number of attached hydrogen atoms. The hydrodynamic volume of each molecule in toluene was theoretically determined from the PCM-B3LYP/6-311G(d,p) calculation. These theoretical values were used to estimate the permanent dipole moment changes under excitations based on experimental data.

Subsequently, to determine the lowest energy one- and two-photon allowed transitions and related molecular parameters of the investigated molecules, the response function calculations[39,40] within the DFT framework were performed using the DALTON program[54]. In this approach, the excitation energies and transition dipole moments (two-photon probabilities) are analytically computed as, respectively, poles and single residues of the linear (quadratic) response function of the molecular electronic density. Moreover, by computing the double residue of the quadratic response function the excited states dipole moments and the transition dipole moment between excited states were also determined. All the response function calculations were performed employing the CAM-B3LYP/6-31+G(d) approach[55] for the investigated molecules in both gas-phase and solvent environment. In the case of the response function calculations, the PCM as implemented in DALTON program was employed[56]. To be consistent, for all molecules the van der Waals surface used in the response function calculations was defined by adopting the set of van der Waals radius and atomic centers determined at the geometry optimization stage using the Gaussian 2009 package.

A preliminary assessment of the exchange-correlation functionals revealed that the standard hybrid B3LYP and PBE0 functionals and also the standard long-range corrected CAM-B3LYP functional, fail to well reproduce the experimental UV-vis spectra of the triarylamine molecules containing trifluoromethyl investigated (for a recent exhaustive summary of TD-DFT benchmarks we refer to excellent reviews[57–59]).

Therefore, in this study the successful strategy of K. Okuno *et al.*[32] of employing a tuned CAM-B3LYP functional was employed. In their systematic study, K. Okuno *et al.*[32] showed that the use of the time-dependent density functional theory (TD-DFT) scheme with the tuned CAM-B3LYP functional is found to semi-quantitatively reproduce several excitation energies identified from the experimental UV–vis spectra of 15 closed forms of diarylethene derivatives. In that study, the default value of the CAM-B3LYP functional parameters, that is $\mu = 0.33$, $\alpha = 0.19$, and $\beta = 0.46$, were tuned to $\mu = 0.150$, $\alpha = 0.0799$ and $\beta = 0.9201$ and the TD-DFT calculations were performed assuming the gas-phase condition. In the present study the values of the functional parameters were defined based on the comparison between the energy of the one-photon lowest-energy transition determined by the PCM/Response function calculation and the energy of the lowest-energy absorption band of the experimental UV–vis spectra of the smallest system investigated, that is, the **H** substituent. Note that in the present study we neglect the zero-point vibrational energy and we compare vertical excitation energy with the experimental absorption band maximum[60]. Here, the following values were adopted as the CAM-B3LYP functional parameters: $\mu = 0.150$, $\alpha = 0.03$ and $\beta = 0.97$. The suitability of such values to the response function calculations addressing the other substituents was confirmed through the satisfactory reproduction of the excitation energy of the lowest-energy transitions (one or two) identified from the experimental UV–vis spectra.

One may point two plausible sources of discrepancies between the values adopted for the CAM-B3LYP functional parameters in the present study and the one by K. Okuno *et al.* The distinct class of compounds investigated is perhaps the main reason. However, another point that can contribute to such differences is that in the present study the values adopted for the CAM-B3LYP functional parameters were determined by performing linear response function calculations in combination with a PCM, while in the work conducted by K. Okuno *et al.* the values were determined based on the results of gas-phase calculations.

Finally, to confirm the donor-acceptor charge transfers involved on the main one- and two-photon transitions of the substitutes, the percentage contribution of the excitations to the transitions, and the KS molecular orbitals involved, were determined. The KS molecular orbitals were determined by DFT calculations using the tuned CAM-B3LYP/6-31+G(d) approach in combination with IEF-PCM and using the Gaussian 2009 package[53].

1. Parthenopoulos, D. A. & Rentzepis, P. M. 3D optical storage memory. *Science* **245**, 843–845 (1989).
2. Corredor, C. C., Huang, Z. L. & Belfield, K. D. Two-photon 3D optical data storage via fluorescence modulation of an efficient fluorene dye by a photochromic diarylethene. *Adv. Mater.* **18**, 2910–2914 (2006).
3. Squirrell, J. M., Wokosin, D. L., White, J. G. & Bavister, B. D. Long-term two-photon fluorescence imaging of mammalian embryos without compromising viability. *Nat. Biotechnol.* **17**, 763–767 (1999).
4. Lazar, J., Bondar, A., Timr, S. & Firestein, S. J. Two-photon polarization microscopy reveals protein structure and function. *Nat. Methods* **8**, 684–690 (2011).
5. Drobizhev, M. *et al.* Primary Role of the Chromophore Bond Length Alternation in Reversible Photoconversion of Red Fluorescence Proteins. *Sci. Rep.* **2**, 688; doi:10.1038/srep00688 (2012).
6. Jacobs, B. C. & Franson, J. D. All-optical switching using the quantum Zeno effect and two-photon absorption. *Phys. Rev. A.* **79**, 063830 (2009).
7. Hendrickson, S. M. *et al.* All-optical-switching demonstration using two-photon absorption and the Zeno effect. *Phys. Rev. A.* **87**, 023808 (2013).
8. Jiang, Y. *et al.* Synthesis, Two-Photon Absorption, and Optical Power Limiting of New Linear and Hyperbranched Conjugated Polyynes Based on Bithiazole and Triphenylamine. *J. Polym. Sci. A1.* **49**, 1830–1839 (2011).
9. Spangler, C. W. Recent development in the design of organic materials for optical power limiting. *J. Mat. Chem.* **9**, 2013–2020 (1999).
10. Baev, A., Norman, P., Henriksson, J. & Agren, H. Theoretical Simulations of clamping levels in optical power limiting. *J. Phys. Chem. B.* **110**, 20912–20916 (2006).
11. Velusamy, M. *et al.* A New Series of Quadrupolar Type Two-Photon Absorption Chromophores Bearing 11,12-Dibutoxydibenzo a,c -phenazine Bridged Amines; Their Applications in Two-Photon Fluorescence Imaging and Two-Photon Photodynamic Therapy. *Adv. Funct. Mater.* **19**, 2388–2397 (2009).
12. Fisher, W. G., Partridge, W. P., Dees, C. & Wachter, E. A. Simultaneous two-photon activation of type-I photodynamic therapy agents. *Photoch. Photobio.* **66**, 141–155 (1997).
13. Sheng, C.-X. *et al.* Ultrafast intersystem-crossing in platinum containing π-conjugated polymers with tunable spin-orbit coupling. *Sci. Rep.* **3**, 2653 (2013).
14. He, G. S., Yuan, L. X., Cui, Y. P., Li, M. & Prasad, P. N. Studies of two-photon pumped frequency-upconverted lasing properties of a new dye material. *J. Appl. Phys.* **81**, 2529–2537 (1997).
15. Ferreira, P. H. D. *et al.* Nonlinear spectrum effect on the coherent control of molecular systems. *Opt. Commun.* **284**, 3433–3436 (2011).
16. Dayan, B., Pe'er, A., Friesem, A. A. & Silberberg, Y. Two photon absorption and coherent control with broadband down-converted light. *Phys. Rev. Lett.* **93** (2004).
17. Cumpston, B. H. *et al.* Two-photon polymerization initiators for three-dimensional optical data storage and microfabrication. *Nature* **398**, 51–54 (1999).
18. Sun, H. B., Matsuo, S. & Misawa, H. Three-dimensional photonic crystal structures achieved with two-photon-absorption photopolymerization of resin. *Appl. Phys. Lett.* **74**, 786–788 (1999).
19. Correa, D. S., Cardoso, M. R., Tribuzi, V., Misoguti, L. & Mendonca, C. R. Femtosecond Laser in Polymeric Materials: Microfabrication of Doped Structures and Micromachining. *IEEE J. Sel. Top. Quant.* **18**, 176–186 (2012).
20. Mendonca, C. R. *et al.* Femtosecond laser waveguide micromachining of PMMA films with azoaromatic chromophores. *Opt. Express* **16**, 200–206 (2008).
21. Albota, M. *et al.* Design of organic molecules with large two-photon absorption cross sections. *Science* **281**, 1653–1656 (1998).
22. De Boni, L., Misoguti, L., Zilio, S. C. & Mendonca, C. R. Degenerate two-photon absorption spectra in azoaromatic compounds. *Chemphyschem* **6**, 1121–1125 (2005).
23. Vivas, M. G. *et al.* Experimental and Theoretical Study on the One- and Two-Photon Absorption Properties of Novel Organic Molecules Based on Phenylacetylene and Azoaromatic Moieties. *J. Phys. Chem. B* **116**, 14677–14688 (2012).
24. Barzoukas, M. & Blanchard-Desce, M. Molecular engineering of push-pull dipolar and quadrupolar molecules for two-photon absorption: A multivalence-bond states approach. *J. Chem. Phys.* **113**, 3951–3959 (2000).
25. Zojer, E. *et al.* Tuning the two-photon absorption response of quadrupolar organic molecules. *J. Chem. Phys.* **116**, 3646–3658 (2002).
26. Zojer, E., Beljonne, D., Pacher, P. & Bredas, J. L. Two-photon absorption in quadrupolar pi-conjugated molecules: Influence of the nature of the conjugated bridge and the donor-acceptor separation. *Chem-Eur J* **10**, 2668–2680 (2004).
27. Beljonne, D. *et al.* Role of dimensionality on the two-photon absorption response of conjugated molecules: The case of octupolar compounds. *Adv. Funct. Mater.* **12**, 631–641 (2002).
28. Hrobarik, P. *et al.* Benzothiazoles with Tunable Electron-Withdrawing Strength and Reverse Polarity: A Route to Triphenylamine-Based Chromophores with Enhanced Two-Photon Absorption. *J. Org. Chem.* **76**, 8726–8736 (2011).
29. Katan, C. *et al.* Effects of (multi)branching of dipolar chromophores on photophysical properties and two-photon absorption. *J. Phys. Chem. A.* **109**, 3024–3037, doi:10.1021/jp044193e (2005).
30. Lee, W. H. *et al.* Two-photon absorption and nonlinear optical properties of octupolar molecules. *J. Am. Chem. Soc.* **123**, 10658–10667 (2001).
31. Liu, K., Wang, Y., Tu, Y., Agren, H. & Luo, Y. Aggregation effects on two-photon absorption spectra of octupolar molecules. *J. Chem. Phys.* **127** (2007).
32. Liu, K., Wang, Y., Tu, Y., Agren, H. & Luo, Y. Two-photon absorption of hydrogen-bonded octupolar molecule clusters. *J. Phys. Chem. B.* **112**, 4387–4392 (2008).
33. Ishow, E. *et al.* Two-photon fluorescent holographic rewritable micropatterning. *J. Am. Chem. Soc.* **129**, 8970–8971 (2007).
34. Jacquart, A., Tauc, P., Pansu, R. B. & Ishow, E. Tunable emissive thin films through ICT photodisruption of nitro-substituted triarylamines. *Chem. Commun.* **46**, 4360–4362 (2010).
35. Ning, Z. & Tian, H. Triarylamine: a promising core unit for efficient photovoltaic materials. *Chem. Commun.* **37**, 5483–5495 (2009).
36. Fang, Z., Webster, R. D., Samoc, M. & Lai, Y.-H. Tuning two-photon absorption cross-sections for triphenylamine derivatives. *RSC adv.* **3**, 17914–17917 (2013).
37. Purser, S., Moore, P. R., Swallow, S. & Gouverneur, V. Fluorine in medicinal chemistry. *Chem. Soc. Rev.* **37**, 320–330 (2008).
38. Salek, P. *et al.* Calculations of two-photon absorption cross sections by means of density-functional theory. *Chem. Phys. Lett.* **374**, 446–452 (2003).
39. Salek, P., Vahtras, O., Helgaker, T. & Agren, H. Density-functional theory of linear and nonlinear time-dependent molecular properties. *J. Chem. Phys.* **117**, 9630–9645 (2002).
40. Ishow, E., Guillot, R., Buntinx, G. & Poizat, O. Photoinduced intramolecular charge-transfer dynamics of a red-emitting dicyanovinyl-based triarylamine dye in solution. *J. Photoch. Photobio. A.* **234**, 27–36 (2012).

41. Ishow, E. *et al.* Multicolor Emission of Small Molecule-Based Amorphous Thin Films and Nanoparticles with a Single Excitation Wavelength. *Chem. Mater.* **20**, 6597–6599 (2008).
42. Ishow, E. *et al.* Comprehensive investigation of the excited-state dynamics of push-pull triphenylamine dyes as models for photonic applications. *Phys. Chem. Chem. Phys.* **15**, 13922–13939 (2013).
43. Suppan, P. Solvatochromic shifts - the influence of the medium on the energy of electronic states. *J. Photoch. Photobio. A.* **50**, 293–330, doi:10.1016/1010-6030(90)87021-3 (1990).
44. Makarov, N. S. *et al.* Impact of Electronic Coupling, Symmetry, and Planarization on One- and Two-Photon Properties of Triarylamines with One, Two, or Three Diarylboryl Acceptors. *J. Phys. Chem. A.* **116**, 3781–3793 (2012).
45. Vivas, M. G. *et al.* Revealing the Electronic and Molecular Structure of Randomly Oriented Molecules by Polarized Two-Photon Spectroscopy. *J. Phys. Chem. Lett.* **4** (2013).
46. Drobizhev, M. *et al.* Strong two-photon absorption in new asymmetrically substituted porphyrins: Interference between charge-transfer and intermediate-resonance pathways. *J. Phys. Chem. B.* **110** (2006).
47. Johnsen, M. *et al.* Effects of conjugation length and resonance enhancement on two-photon absorption in phenylene–vinylene oligomers. *Phys. Chem. Chem. Phys.* **10**, 1177–1191 (2008).
48. Macak, P., Luo, Y., Norman, P. & Agren, H. Electronic and vibronic contributions to two-photon absorption of molecules with multi-branched structures. *J. Chem. Phys.* **113**, 7055–7061 (2000).
49. Bonin, K. D. & McIlrath, T. J. Two-photon electric-dipole selection rules. *J. Opt. Soc. Am. B.* **1**, 52–55 (1984).
50. Becke, A. D. Density-functional exchange-energy approximation with correct asymptotic-behavior. *Phys. Rev. A.* **38**, 3098–3100 (1988).
51. Lee, C. T., Yang, W. T. & Parr, R. G. Development of the colle-salvetti correlation-energy formula into a functional of the electron-density. *Phys. Rev. B.* **37**, 785–789 (1988).
52. Frisch, M. J., Pople, J. A. & Binkley, J. S. Self-consistent molecular-orbital methods 25. Supplementary functions for Gaussian basis sets. *J. Chem. Phys.* **80**, 3265–3269 (1984).
53. Frisch, M. J. *et al.* (2009, revision D1).
54. A molecular electronic structure program, Release 2.0 (2011), see http://www.kjemi.uio.no/software/dalton/dalton.html, last accessed at 1/21/2014 (2011).
55. Yanai, T., Tew, D. P. & Handy, N. C. A new hybrid exchange-correlation functional using the Coulomb-attenuating method (CAM-B3LYP). *Chem. Phys. Lett.* **393**, 51–57 (2004).
56. Frediani, L., Rinkevicius, Z. & Agren, H. Two-photon absorption in solution by means of time-dependent density-functional theory and the polarizable continuum model. *J. Chem. Phys.* **122** (2005).
57. Jacquemin, D. *et al.* TD-DFT Performance for the Visible Absorption Spectra of Organic Dyes: Conventional versus Long-Range Hybrids. *J. Chem. Theory Comp.* **4**, 123–135 (2007).
58. Jacquemin, D. *et al.* Extensive TD-DFT Benchmark: Singlet-Excited States of Organic Molecules. *J. Chem. Theory Comp.* **5**, 2420–2435 (2009).
59. Charaf-Eddin, A. *et al.* Choosing a Functional for Computing Absorption and Fluorescence Band Shapes with TD-DFT. *J. Chem. Theory Comp.* **9**, 2749–2760 (2013).
60. Lasorne, B. *et al.* Vertical transition energies vs. absorption maxima: Illustration with the UV absorption spectrum of ethylene. *Spectrochim Acta A Mol Biomol Spectrosc* **119**, 52–58 (2014).

Acknowledgments

Financial support from FAPESP (Fundação de Amparo à Pesquisa do estado de São Paulo, processo nº: 2011/12399-0 e nº: 2009/11810-8), CNPq (Conselho Nacional de Desenvolvimento Científico e Tecnológico), Coordenação de Aperfeiçoamento de Pessoal de Nível Superior (CAPES) and the Air Force Office of Scientific Research (FA9550-12-1-0028) are acknowledged. R.Z. is a Wenner-Gren Foundations scholar. This work was also supported by a computational Grant from the Swedish Infrastructure Committee (SNIC) for the Project "Multiphysics Modeling of Molecular Materials" (SNIC 025/12-38).

Author contributions

M.G.V. conceived the idea of this study and performed the nonlinear optical measurements while J.M. and M.B. synthesized the molecules and characterized their linear optical properties. D.L.S., R.Z., W.B. and H.A. performed the quantum chemical calculations. L.D.B., S.C., E.I. and C.R.M. supervised this study. All authors contributed to the writing of this manuscript.

Additional information

Supplementary information accompanies this paper at http://www.nature.com/scientificreports

Competing financial interests: The authors declare no competing financial interests.

How to cite this article: Vivas, M.G. *et al.* Molecular Structure – Optical Property Relationships for a Series of Non-Centrosymmetric Two-photon Absorbing Push-Pull Triarylamine Molecules. *Sci. Rep.* **4**, 4447; DOI:10.1038/srep04447 (2014).